Marine Chemistry 265-266 (2024) 104433

Contents lists available at ScienceDirect

Marine Chemistry

journal homepage: www.elsevier.com/locate/marchem

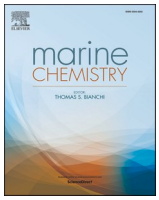

Particulate mercury export in the Central Pacific Ocean using ^{234}Th—^{238}U disequilibria

Blaire P. Umhau [a,*], Laura C. Motta [b], Joel D. Blum [c], Hilary G. Close [d,e], Jeffrey C. Drazen [f], Brian N. Popp [e], Claudia R. Benitez-Nelson [a]

[a] School of Earth, Ocean & Environment, University of South Carolina, 701 Sumter Street, Columbia, SC 29208, USA
[b] Marine Chemistry and Geochemistry, Woods Hole Oceanographic Institution, 266 Woods Hole Road Woods Hole, MA 02543, USA
[c] Department of Earth and Environmental Sciences, University of Michigan, 1100 N University Avenue, Ann Arbor, MI 48109, USA
[d] Rosenstiel School of Marine and Atmospheric Science, University of Miami, 4600 Rickenbacker Causeway, Miami, Florida, 33149, USA
[e] Department of Earth Sciences, University of Hawaii at Manoa, 1680 East West Road, Honolulu, HI 96822, USA
[f] Department of Oceanography, University of Hawaii at Manoa, 1000 Pope Road, Honolulu, HI 96822, USA

ARTICLE INFO

Keywords:
Particle flux
Uranium-238
Thorium-234
Mercury export
Station ALOHA
Equatorial Pacific
Methylmercury
Mercury bioaccumulation

ABSTRACT

Mercury (Hg) is a potent neurotoxin that enters the food web and may contaminate commercial, recreational, subsistence, and ceremonial fish stocks. Understanding the pathways by which this contamination occurs in marine systems is thus an essential component of minimizing consumer health risk. Our knowledge of the biogeochemical cycling of mercury, however, is relatively limited. Temporal changes in sinking particulate mercury (PHg) fluxes throughout the upper 400 m were examined at Station ALOHA (22°N, 158°W) in the North Pacific Subtropical Gyre (NPSG) and spatially along a north-south transect to the Equator (17.5°N to 5°N x 155°W) using a combination of in situ pumps and Uranium-238/Thorium-234 disequilibria as a tracer of particle export. Our results indicate that Station ALOHA is characterized by seasonally variable export fluxes of PHg, with highest fluxes occurring in May (175 m, 346 pmol m^{-2} day^{-1}), with the advent of summer zooplankton growth, and in September (400 m, 356 pmol m^{-2} day^{-1}), coinciding with a diazotroph mediated summer export pulse. PHg fluxes in May and September were higher than those previously measured in the equatorial Pacific at 150 m and continued to be high (> 100 pmol Hg m^{-2} d^{-1}) down to 400 m, thereby providing a significant source of Hg to the mesopelagic food web. In contrast to Station ALOHA, at 8 and 5°N, PHg fluxes attenuated rapidly with depth, and fluxes were generally lower, with a maximum flux of 86 pmol m^{-2} d^{-1} (5°N). Depth profiles at 8 and 5°N were significantly different from one another, with PHg fluxes higher throughout the water column at 5°N and characterized by a subsurface peak in Hg flux 3 times higher than at 8°N (86 vs. 29 pmol Hg m^{-2} d^{-1}). Monomethylmercury (MeHg) fluxes (max = 1.09 ± 0.57 pmol m^{-2} d^{-1}) and concentrations (max = 0.14 fmol L^{-1}) comprised only a small percentage of the total PHg pool. These results suggest that PHg cycling significantly differed between the NPSG and near the equator at least during an El Niño year. At Station ALOHA, microbial reworking of small particles below the deep chlorophyll maximum coupled with changes in zooplankton grazing drive seasonal export variability. In contrast near the equator, low fluxes associated with low biological productivity result in significantly lower PHg transport to depth during an El Niño year.

1. Introduction

Characterizing the magnitude and composition of particles as they sink from the ocean's surface to depth is a critical component of carbon, nutrient, and trace element biogeochemical cycling (Alonso-Gonzalez et al., 2010; Anderson, 2020; Buesseler et al., 2020; Buesseler et al., 2008; Siegel et al., 2016; Volk and Hoffert, 1985). Both small and large particles are important contributors to vertical flux (Kiko et al., 2017; Puigcorbé et al., 2015; Richardson and Jackson, 2007). Small particles play an especially vital role in trace element and isotope scavenging and export due to their high surface area (Lam et al., 2015), and both small and large particles provide a potential food source of carbon, nutrients and trace elements to higher trophic levels (Alonso-Gonzalez et al., 2010; Choy et al., 2015; Durkin et al., 2015; Hannides et al., 2020; Lam

* Corresponding author.
E-mail address: b.umhau@earth.miami.edu (B.P. Umhau).

https://doi.org/10.1016/j.marchem.2024.104433
Received 2 April 2024; Received in revised form 18 June 2024; Accepted 21 July 2024
Available online 24 July 2024

et al., 2015; Puigcorbé et al., 2015; Steinberg et al., 2008; Umhau et al., 2019; Romero-Romero et al., 2020). As such, scavenging and biologically mediated uptake of dissolved seawater constituents onto and into particles is a significant mechanism for the introduction and subsequent bioaccumulation of trace elements in marine biota (Lam et al., 2015; Lamborg et al., 2016; Sunderland et al., 2018).

Trace metal mercury (Hg) cycles through several forms in the marine environment. It is deposited from the atmosphere into the surface ocean predominantly as Hg^{2+}, where it may be reduced and methylated into the highly toxic forms monomethylmercury (MeHg) and dimethylmercury (DMHg). MeHg bioaccumulates and is biomagnified in higher trophic levels. Therefore, predatory fish that are harvested for human consumption via commercial, recreational, subsistence, and ceremonial fishing, are a primary source of human exposure to Hg (Fitzgerald et al., 2007; Fitzgerald and Lamborg, 2003; Lamborg et al., 2016; Selin, 2009). Like many other trace elements, Hg is highly particle reactive and is rapidly scavenged onto particles. Thus particle export to depth is a major removal mechanism of Hg from the upper ocean (e.g., Lamborg et al., 2016; Washburn et al., 2019).

Several studies suggest that surface water Hg concentrations have been enriched over time due to the cumulative inputs from anthropogenic emissions (Horowitz et al., 2014; Lamborg et al., 2014a; Lamborg et al., 2014b; Streets et al., 2019). Yet, maximum open ocean MeHg concentrations are typically found below the depth of the mixed layer, at depths exceeding 100 m, and in low oxygen zones (Blum et al., 2013; Cossa et al., 2011, Cossa et al., 2009; Hammerschmidt and Bowman, 2012; Laurier et al., 2004; Mason and Fitzgerald, 1993; Mason and Sullivan, 1999; Munson et al., 2015; Sunderland et al., 2009). Indeed, lab and field measurements suggest that a significant proportion of MeHg is demethylated into inorganic and gaseous forms via photochemical reactions in the surface ocean (Black et al., 2012; DiMento and Mason, 2017; Fernández-Gómez et al., 2013; Jeremiason et al., 2014; Motta et al., 2019; Motta et al., 2022).

Combined, these observations suggest that the downward transport of sinking particles and subsurface biochemical reactions are likely important pathways of Hg incorporation into the mesopelagic marine food web (Cossa et al., 2012; Motta et al., 2022). Higher MeHg concentrations at depth have been directly attributed to biotic methylation of Hg(II) in marine particles (Blum et al., 2013; Cossa et al., 2011; Sunderland et al., 2009). Choy et al. (2009) found that Hg concentrations in pelagic fish increased with depth. More recently, Motta et al. (2022) found that MeHg is likely produced preferentially in situ in small particles below the euphotic zone, but above 400 m. Motta et al. (2019) used Hg isotopic signatures to argue that MeHg formed at depth is directly incorporated into the food web via zooplankton grazing, with particles enriched in Hg providing another source to zooplankton and higher trophic levels at depth. Unfortunately, information regarding the particulate flux and transformations of Hg in the water column remains limited (Lamborg et al., 2016).

Thorium-234 ($t_{½}$ = 24.1 d) is produced by the radioactive decay of ^{238}U ($t^{½}$ = 4.47 × 10^9 y) in seawater. Since ^{234}Th is highly particle reactive, it is rapidly scavenged onto particles, and released when particles are remineralized. The disequilibrium from its soluble conservative parent, ^{238}U, thus provides information on where particle export (^{234}Th deficiency due to scavenging onto sinking particles) and remineralization (^{234}Th excess due to solubilization or fragmentation) occurs on timescales of days to weeks (Benitez-Nelson et al., 2001b; Buesseler et al., 2009; Coale and Bruland, 1985; Maiti et al., 2010). This method has been used to calculate residence times and sinking particulate fluxes of carbon, nutrients (Buesseler et al., 2009; Haskell et al., 2013; Owens et al., 2015), and a suite of trace metals, including Hg (Lamborg et al., 2016; Tesan Onrubia et al., 2020; Weinstein and Moran, 2005) with high vertical resolution (Owens et al., 2015).

Here, we used ^{234}Th- ^{238}U disequilibria to quantify sinking Hg export fluxes seasonally at Station ALOHA, located in the North Pacific Subtropical Gyre (NPSG), and spatially along a north-south transect from the Hawaiian Islands to the Equator (Fig. 1). Total particulate Hg (PHg) and a limited number of particulate MeHg measurements were made on small and large particles collected using in situ pumps. Mercury fluxes are discussed in the context of particulate carbon export, and bulk Hg, Hg isotope, and amino acid $\delta^{15}N$ values of particles, zooplankton, and micronekton that were collected concurrently and are discussed in detail elsewhere (Gloeckler et al., 2018; Hannides et al., 2020; Motta et al., 2019, 2022; Umhau et al., 2019).

2. Study area

Station ALOHA (22°N, 158°W) is the site of the long-running Hawaiian Ocean Time-series (HOT) program and is often used to constrain processes that occur throughout the entire NPSG (Grabowski et al., 2019; Karl and Lukas, 1996; Kavanaugh et al., 2018). While the thermocline and halocline remain relatively stable throughout the year, this site experiences a seasonal increase in particle export mediated by diazatrophs in the late summer that delivers material to the deep ocean at rates up to three times higher than those measured at other times of the year (Böttjer et al., 2017; Karl et al., 2012; Umhau et al., 2019). Sampling was conducted in February 2014, September 2014, and May 2015, representing seasons previously identified as having respectively low, high, and intermediate productivity and hence particle flux (Karl et al., 2012; Umhau et al., 2019). Additional samples were collected along a N-S transect along 155°W from low productivity waters at 17.5°N to higher productivity waters at 5°N and across a shoaling of the oxygen minimum zone from below 400 m (17.5°N) to 130 m (10°N). During sampling in August 2015, the region was impacted by strong El Niño conditions (https://origin.cpc.ncep.noaa.gov/products/analysis_monitoring/ensostuff/ONI_v5.php).

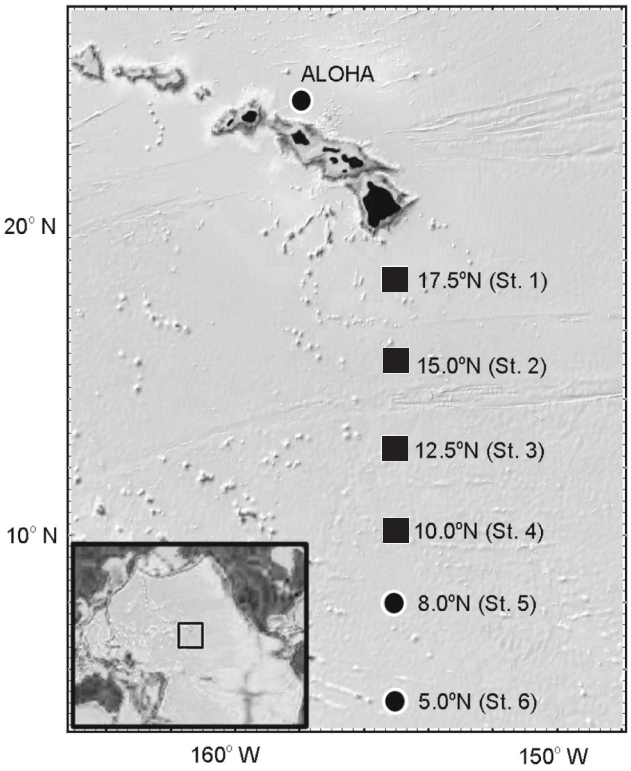

Fig. 1. Map of sampling station locations. Adapted from Umhau et al. (2019).

3. Methods

3.1. Sample collection

Samples were collected using the R/V *Kilo Moana* over a seasonal cycle at Station ALOHA during cruises ranging from ten to fourteen days in February 2014, September 2014, and May 2015. In August–September 2015, additional samples were collected at six stations along a transect from 17.5°N to 5°N at 155°W. Stations 1–4 (17.5°, 15°, 12.5° and 10°N) were occupied for approximately four hours, with water column samples collected over the upper 400 m using Niskin bottles attached to a CTD Rosette, and particles were collected at 150 m using two in situ pumps (WTS-LV McLane Research Laboratories). Stations 5 (8°N) and 6 (5°N) were occupied for nine days each (Fig. 1). As such, multiple in situ pump casts were completed several times at 8°N and 5°N and at Station ALOHA, enabling full depth profiles of small (1–53 μm) and large (>53 μm) particles to be collected at these sites. While one CTD cast was used to collect water samples at Stations 1–4, several CTD casts were used to collect water samples from 8°N and 5°N as well as at Station ALOHA. A Seabird SBE 9/11plus CTD was deployed with two Sea-Bird SBE 3P temperature sensors, two Sea-Bird SBE 4C conductivity sensors, two Sea-Bird SBE 43 dissolved oxygen sensors, and a Wetlabs ECO FLNTU Chlorophyll Fluorometer and Turbidity sensor, providing measurements of salinity, temperature, fluorescence, photosynthetically active radiation (PAR) and dissolved oxygen.

Particulate sample collection methods are detailed in Motta et al. (2019) and in Umhau et al. (2019). Briefly, 142 mm diameter, 1 μm pore-size QMA filters and 53 μm pore-size Nitex filters were cleaned according to the trace metal clean protocols described in detail by Umhau et al. (2019) and Motta et al. (2019, 2022). Filters were mounted sequentially by size on metal-free mini-MLVFS filter holders attached to the in situ pumps and deployed at depths between 10 and 400 m (N = 2–11 depths) depending on the station (Lam et al., 2015; Umhau et al., 2019). Between ~600–2000 L of water were filtered per deployment at a rate of 8 L min^{-1}. High flow rates of ~20 L min^{-1} were used to filter large volumes of water (~ 5000–7000 L, N = 16) required for capturing sufficient >53 μm particles for isotopic and compound specific analyses (Motta et al., 2019, 2022).

3.2. Total ^{234}Th

Total ^{234}Th sampling and analyses are similar to those described in Buesseler et al. (2001) and Benitez-Nelson et al. (2001b), with primary data from this study published in Umhau et al. (2019). Briefly, 2 L of seawater was collected from 5 to 400 m (N = 11–14). Samples were acidified to pH ~ 1 and a ^{230}Th yield tracer added. After samples were allowed to equilibrate for 6–8 h, the pH was adjusted to ~8–9, and reagents added to form a Mn-oxide precipitate that scavenges Th. Samples were allowed to stand for ~8 h; after which the precipitate was filtered onto a 25 mm quartz microfiber filter (QMA) and dried at 60 °C before counting on a low level RISO beta counter. Samples were recounted after six months to account for any residual background activity stemming from other naturally occurring radionuclides that co-precipitate with the Mn-oxide. ^{230}Th sample recoveries were measured using ICP-MS after acid digestion according to the methods described in Pike et al. (2005) and detailed in Umhau et al. (2019).

3.3. Particle analyses

Small particles collected using QMA filters were subsampled in triplicate using a ~ 25 mm Delrin punch for particulate ^{234}Th, total carbon (C) and bulk C and nitrogen (N) isotopic analyses under trace metal clean conditions, with the remaining filter saved for Hg analyses. All C, N, and Hg filters were stored frozen at −80 °C. Large particle (> 53 μm) samples for ^{234}Th, C, and bulk N were rinsed onto 25 mm QMA filters using 0.2 μm filtered seawater and visible swimmers were removed. Samples were then dried, mounted onto RISO discs, and stored at 4 °C prior to and immediately following counting. Large particle samples for Hg analyses were collected on separate deployments (3000–8000 L filtered) and frozen whole in trace metal clean petri dishes for PHg, MeHg and Hg isotopic analyses. In some cases, it was necessary to combine multiple filters (N = 2–10 filters) from repeat pump deployments over a 10 m depth range to obtain enough material for analysis. Isotopic and dissolved Hg data are discussed in detail in Motta et al. (2019, 2022).

All PHg samples were measured at the University of Michigan according to the methods described in Motta et al. (2019) and Biswas et al. (2008). Briefly, particles on the 25 mm QMA filters underwent a two-step combustion-oxidation process and/or microwave assisted digestion prior to total PHg analysis by cold vapor atomic absorption spectroscopy (CV-AAS) (Motta et al., 2019, 2022). Due to the large quantity of material required to measure MeHg, this component of the dataset is more limited (N = 6). MeHg concentrations on small particles were determined by digesting filter subsamples (three 25 mm punches per digestion) in 2 N trace metal clean HNO_3 for six hours at 60 °C with sonication before and after the digestion (Munson et al., 2015). There is no reference standard for digesting marine particles for MeHg content, so reference TORT-3: Lobster Hepatopancreas Reference Material (NRC) was used. TORT-3 is approximately 50% Hg(II) and 50% MeHg. TORT-3 was digested twice, and each digest was measured twice (recovery = 103%; 0.02 2SD; n = 4 measurements). It should be noted that the error of the measurement is 11% (2SD) from the routine check standard during the analysis (Motta et al., 2019). In deployments where pumps malfunctioned and no water was actively filtered (pumps failed to turn on), filters were used as THg and MeHg process blanks. For the small particles, subsample THg blanks (N = 4) averaged 0.2% of THg concentrations. For the large particles, after post-processing onto 47 mm QMA filters, THg blanks averaged 0.4% (N = 3) of THg concentrations. All MeHg blanks were below the instrument detection limit.

Particulate carbon and nitrogen measurements were made according to the methods described in Kennedy et al. (2005) and Umhau et al. (2019) at the University of Hawaii at Manoa. Samples were dried overnight at 60 °C, encapsulated into tin cups, and analyzed using an isotope ratio mass spectrometer (IRMS; DeltaPlus XP) coupled to an elemental analyzer (Conflo IV/Costech ECS 4010). Supplementary data on the carbon and nitrogen contents, δ^{15}N of amino acid composition on particles, as well as zooplankton and nekton biomass collected during these cruises are discussed in detail by Umhau et al. (2019), Gloeckler et al. (2018) Hannides et al. (2020) and Romero-Romero et al. (2020), respectively.

3.4. Particle fluxes derived using ^{234}Th

Thorium-234 derived sinking particle fluxes were determined using a 1D steady state model as described in Umhau et al. (2019). Physical processes are assumed to be negligible at Station ALOHA as there was no evidence of mesoscale features during sample collection and it has been shown that differences between steady state and non-steady state measurements are minimal (Benitez-Nelson et al., 2001a; Benitez-Nelson et al., 2001b; Buesseler et al., 2009). Along the N-S transect, physical processes were also assumed to be small. This is consistent with previous work and the strong El Niño conditions at the time of sampling (Bacon et al., 1996; Buesseler et al., 1995; Umhau et al., 2019). Fluxes of ^{234}Th were calculated by subtracting the activity of ^{234}Th from the activity of ^{238}U determined from salinity using the equation of Owens et al. (2011) and integrating over the depth horizons of interest (See Umhau et al., 2019). Small and large particle Hg (and C) to ^{234}Th ratios measured at the depth horizon of interest were then multiplied by the ^{234}Th flux to determine ^{234}Th derived fluxes of PHg throughout the water column (Buesseler et al., 2006). In some instances, calculated fluxes were negative. These fluxes are reported here as “below detection” as error bars were large and overlapped with zero.

4. Results

4.1. Oxygen, fluorescence, temperature and salinity

Seasonal variations in salinity, temperature, and oxygen at the oligotrophic time series site, Station ALOHA, were minimal (Buesseler et al., 2008; Church et al., 2013) and oxygen concentrations decreased from ~200 μmol kg^{-1} at the surface to 160–170 μmol kg^{-1} at 400 m. Along the transect, the depth of the oxygen minimum zone (< 30 μmol kg^{-1}) shoaled with decreasing latitude from a depth of 700 m at Station ALOHA to a depth of 130 m at 8°N, before deepening back below 400 m at 5°N. Mixed layer depths at Station ALOHA varied seasonally, from 100 m in February to 45 m in May and September. Along the transect, the mixed layer was shallowest at 25 m at 15°N and 12.5°N, deepening to 60 m at 5°N. Station ALOHA was characterized by fluorescence maxima at ~125 m across all three seasons (0.4 to ~1.0 mg m^{-3}), with

Table 1
Concentrations of particulate total mercury (PHg), ratios of PHg to thorium (PHg/Th), fluxes of PHg, and PHg to particulate carbon (PHg/PC) in the 1–53 μm size fraction. BD indicates fluxes that are within error of zero.

(1-53 μm)	PTh	(±)	PHg	(±)	PHg/PTh	(±)	PHg flux	(±)	PHg/PC	(±)
Depth (m)	(dpm L^{-1})	Error	(fmol L^{-1})	Error	(fmol dpm^{-1})	Error	(pmol m^{-2} d^{-1})	Error	(fmol $nmol^{-1}$)	Error
Feb. 2014										
St. ALOHA										
25	0.12	0.01	72	3.6	600	51	75	7	0.08	0.009
50	0.16	0.01	67	3.3	419	432	45	7	0.08	0.009
75	0.24	0.02	70	3.5	292	285	14	4	0.10	0.011
150	0.18	0.01	39	2.0	217	216	90	8	0.09	0.011
175	0.15	0.01	29	1.5	193	200	115	11	0.12	0.013
200	0.16	0.01	42	2.1	263	266	93	11	0.16	0.018
400	0.14	0.01	26	1.3	186	189	BD	BD	0.14	0.016
Sept. 2014										
St. ALOHA										
25	0.12	0.01	87	9	725	121	22	7	0.06	0.008
50	0.11	0.02	82	8	745	119	86	25	0.06	0.009
100	0.12	0.02	38	4	317	54	84	18	0.05	0.007
125	0.11	0.01	25	3	227	28	106	18	0.05	0.006
150	0.12	0.01	29	3	242	39	143	28	0.07	0.010
175	0.14	0.02	25	3	179	29	122	21	0.11	0.015
200	0.14	0.02	28	3	200	35	167	37	0.10	0.014
250	0.13	0.01	27	3	208	26	237	38	0.11	0.016
400	0.10	0.01	23	2	230	38	356	75	0.11	0.016
May 2015										
St. ALOHA										
25	0.14	0.02	58	6	414	67	32	8	0.06	0.009
50	0.19	0.02	54	5	284	42	68	11	0.06	0.008
75	0.24	0.04	67	7	279	52	75	15	0.08	0.011
125	0.22	0.03								
150	0.21	0.03	25	3	119	18	82	15	0.06	0.008
175	0.08	0.01	43	4	538	61	346	60	0.20	0.028
200	0.15	0.01	37	4	247	34	153	20	0.13	0.020
250	0.16	0.02	29	3	181	58	108	19	0.12	0.017
400	0.07	0.02	22	2	314	111	257	81	0.12	0.017
Sept. 2015										
17.5°N										
150	0.13	0.02	10	1	77	12	BD	BD	0.02	0.002
10°N										
150	0.13	0.02	27	3	208	34	9	39	0.09	0.010
8°N										
5	0.48	0.06	88	9	183	30	2	3	0.15	0.017
25	0.36	0.04	84	8	233	33	21	15	0.12	0.013
50	0.31	0.04	46	5	148	24	31	12	0.02	0.002
100	0.25	0.02	36	4	144	19	29	12		
125	0.19	0.02	38	4	200	31	29	19	0.11	0.013
150	0.21	0.02	24	2	114	16	7	11	0.08	0.009
175	0.21	0.02	19	2	90	13	BD	BD		
250	0.19	0.01	26	3	137	17	BD	BD	0.14	0.016
400	0.15	0.01	24	2	160	20	41	87	0.10	0.011
5°N										
5	0.72	0.06	22	2	31	4	3	5	0.02	0.002
25	0.45	0.08	66	7	147	29	39	23	0.06	0.007
50	0.24	0.01	36	4	150	17	38	23	0.04	0.004
100	0.23	0.02	44	4	191	27	86	37	0.05	0.006
150	0.21	0.03	24	2	114	19	44	23	0.06	0.007
250	0.18	0.02	23	2	128	18	18	27	0.08	0.009
300	0.18	0.02	30	3	167	24	BD	BD	0.12	0.014
400	0.13	0.01	28	3	215	32	BD	BD	0.13	0.015

highest fluorescence measured in September. Along the transect stations, however, fluorescence never exceeded ~0.6 mg m^{-3} and shoaled by ~50 m from the 100–150 m observed in the north. The shallowest fluorescence maximum occurred at 8°N at 75 m across the oxygen transition zone.

4.2. Total ^{234}Th and ^{234}Th derived sinking particle fluxes

All water column ^{234}Th activities (dpm L^{-1}) are reported in detail in Umhau et al. (2019). In general, total ^{234}Th activities were high and close to equilibrium with ^{238}U, resulting in low ^{234}Th deficits and thus low sinking particle fluxes. ^{234}Th activities were generally lowest at Station ALOHA and increased (i.e., closer to equilibrium with ^{238}U) along the transect stations. Seasonal differences occurred at Station ALOHA; in September, ^{234}Th activities were consistently low throughout the upper 150 m of the water column, whereas in February and May, activities were higher, with deeper depths occasionally characterized by ^{234}Th activity in excess of ^{238}U activity, indicative of particle remineralization. Along transect stations (5°-17.5°N), ^{234}Th activities were high, and generally equal to or higher (within error) than ^{238}U activities by 150 m, again indicating negligible particle export during sampling (Umhau et al., 2019).

Thorium fluxes derived from ^{234}Th and ^{238}U disequilibrium are described in detail in Umhau et al. (2019) using a 1D steady state model (See section 2.3). ^{234}Th fluxes at Station ALOHA were lowest in February and highest in September and ranged from below detection to 1546 dpm m^{-2} day^{-1} (Umhau et al., 2019).

4.3. Particle concentrations

All small (1–53 μm) and large (> 53 μm) particulate ^{234}Th activities (dpm L^{-1}) and particulate carbon (PC) concentrations are reported in detail in Umhau et al. (2019). Briefly, at Station ALOHA small and large PC concentrations were highest in September (1528 nmol L^{-1} and 148 nmol L^{-1}, respectively), and lowest in May and February, with highest PC concentrations at the surface that decreased with increasing depth. Differences among seasons and trends with depth were more pronounced in the large versus small particle size fraction. At 8° and 5°N, small PC profiles are characterized by sub-surface peaks at 50 and 75 m, respectively, before decreasing with increasing depth. Highest large particle PC concentrations of 166 nmol L^{-1} were measured at 125 m at 5°N, although they were considerably lower than the small particle PC maxima, and concentrations decreased only minimally with increasing In general, at Station ALOHA, there were no seasonal differences in ^{234}Th activities in small and large particles (Tables 1 and 2).

Small total particle mercury concentrations were generally highest over the upper 25 m across all stations (73 ± 13 fmol L^{-1}), with a sharp decline below 75 m at Station ALOHA and 50 m at 5° and 8° N, followed by a more gradual decline with increasing depth to <28 fmol L^{-1} by 400 m (Table 1, Fig. 2). Highest concentrations were measured in the upper 75 m in September, followed by February and May. Along the transect stations at 5°N, small particle Hg concentrations were characterized by a subsurface peak at 25 m of 66 fmol L^{-1}, prior to declining with depth below 150 m. Due to the large volume of water required to obtain measurements, large particle Hg concentrations results are limited. Large particle Hg concentrations at both Station ALOHA and along the transect stations were an order of magnitude lower than those measured in the smaller particle fraction with no discernible trends with depth or season and averaged 3 ± 2 fmol L^{-1}. While small particle Hg concentrations at 5°N were consistently on the lower end of the PHg concentrations measured, large particle Hg concentrations at this site were among the highest (Fig. 2).

Concentrations of MeHg on small and large particles were measured on a limited number of samples and were 0.5% to 4% of the total PHg concentration. The highest MeHg concentration of 0.14 fmol L^{-1} was measured on small particles at 200 m at 5°N, while the lowest concentration of 0.01 fmol L^{-1} was measured on large particles at 25 m at 8°N (Table 3).

4.4. Elemental ratios

At Station ALOHA, small particle PHg/Th ratios varied seasonally over the upper 200 m, with differences driven almost entirely by changes in PHg concentrations (Table 1); particulate ^{234}Th activities remained relatively constant. Highest surface water ratios occurred in September (725 fmol dpm^{-1}), decreased in February (600 fmol dpm^{-1}),

Table 2
Concentrations of particulate total mercury (PHg), ratios of PHg to thorium (PHg/Th), fluxes of PHg, and PHg to particulate carbon (PHg/PC) in the >53 μm size fraction. BD indicates fluxes that are within error of zero.

> 53 μm	PTh	(±)	PHg	(±)	PHg/PTh	(±)	PHg flux	(±)	PHg/PC	(±)
Depth (m)	(dpm L^{-1})	Error	(fmol L^{-1})	Error	(fmol dpm^{-1})	Error	(pmol m^{-2} d^{-1})	Error	(fmol $nmol^{-1}$)	Error
Feb. 2014										
St. ALOHA										
25	0.005	0.0003	3	0.32	600	61	75	10	0.04	0.004
400	0.0100	0.0006	1	0.14	100	11	BD	BD	0.06	0.007
Sept. 2014										
St. ALOHA										
150	0.028	0.0026	1	0.08	36	4	21	3	0.01	0.001
May 2015										
St. ALOHA										
25	0.011	0.0005	1	0.12	91	13	7	1	0.01	0.001
150	0.013	0.0005	3	0.33	231	27	160	19	0.05	0.007
Sept. 2015										
8°N										
25	0.236	0.0134	2	0.10	8	1	1	1	0.04	0.003
100	0.064	0.0123	4	0.20	63	12	13	5	0.14	0.010
150	0.034	0.0076	2	0.20	59	14	3	6	0.04	0.029
5°N										
25	0.012	0.0010	3	0.15	250	24	67	38	0.10	0.007
100	0.021	0.0016	7	0.37	333	32	150	64	0.11	0.008
150	0.039	0.0047	4	0.19	103	13	40	19	0.11	0.007
400	0.011	0.0008	2	0.08	182	13	BD	BD	0.11	0.006

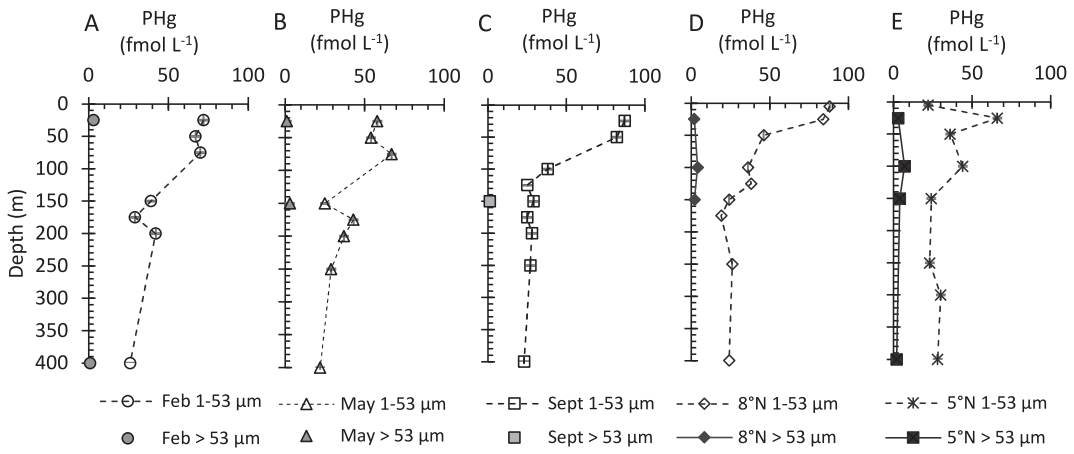

Fig. 2. Plots of particulate mercury (PHg) concentration with depth for small (1–53 µm) and large (> 53 µm) particles derived using 238 U-234Th disequillibria and in-situ pumps. Small and large particulate Hg concentrations collected from Station ALOHA in February are shown in panel A; May data from Station ALOHA are plotted in panel B. Data collected at Station ALOHA in September are shown in panel C, and panels D and E depict data from 8°N and 5°N respectivley along 155°W. Error bars indicate standard error and in some cases are smaller than the symbol.

Table 3
Concentrations of particulate monomethyl mercury (MeHg), ratios of MeHg to thorium (MeHg/Th), and fluxes of MeHg in both size fractions. *150 m MeHg concentration is the average of samples taken at 140 m and 165 m. BD indicates fluxes that are within error of zero.

Size Class	Station Location	Depth	MeHg	(±)	MeHg/Th	(±)	MeHg flux	(±)	MeHg/PC	(±)
	Sept. 2015	(m)	(fmol L^{-1})	Error	(fmol dpm^{-1})	Error	(pmol m^{-2} d^{-1})	Error	fmol $nmol^{-1}$	Error
(1-53 µm)	8°N	200	0.07	0.010	0.35	0.05	BD	BD	0.0003	0.00004
	5°N	150	0.10	0.010	0.48	0.08	0.18	0.09	0.0003	0.00003
		200	0.14	0.014	0.61	0.10	0.18	0.12	0.0004	0.00005
(>53 µm)	8°N	25	0.01	0.001	0.04	0.03	BD	BD	0.0002	0.00002
		150	0.02	0.002	0.59	1.14	0.03	0.07	0.0004	0.00028
		200	0.08	0.010	3.58	5.49	BD	BD	0.0024	0.00034
	5°N	25	0.02	0.002	1.67	0.17	0.45	0.21	0.0007	0.00007
		150*	0.11	0.011	2.82	0.46	1.09	0.57	0.0029	0.00033

and were lowest in May (414 fmol dpm^{-1}). Small particle PHg/Th ratios declined with increasing depth in the water column, stabilizing to an average of 214 ± 48 fmol dpm^{-1} between 150 and 400 m, with the exception of a subsurface PHg/Th peak at 175 m in May (Fig. 3). Large particle PHg/Th ratios were often lower than those measured in small particles and ranged from 36 to 600 fmol dpm^{-1}. Given the limited PHg data on large particles, there were no significant seasonal and depth trends detected (Table 2).

Small and large particulate PHg/Th ratios measured at the transect stations were lower and showed small variations driven by Hg concentration. Over the upper 150 m, small particle PHg/Th ratios ranged from 31 to 233 fmol dpm^{-1} (Table 1). Between 150 and 400 m, ratios declined and remained relatively constant, averaging 147 ± 36 fmol dpm^{-1} and were similar, on average, to those measured in large particles (102 ± 57). Given the limited PHg data on large particles, it is impossible to discern significant depth or latitudinal trends; the large particle PHg/Th ratio was highest at 100 m at 5°N (333 fmol dpm^{-1}) and lowest at 8°N at 25 m (8 fmol dpm^{-1}). Ratios of MeHg/Th ranged from 0.04 to 3.58 fmol dpm^{-1} where data are available (Table 3).

To determine potential differences in bioaccumulation versus surface adsorption, we examined PHg to PC ratios. At Station ALOHA, ratios of PHg/PC on small particles are relatively constant over the upper 150 m, with significantly higher ratios measured in February (*t*-test, $p < 0.05$) relative to May and September. Much of this difference is driven by seasonal changes in PC concentrations. In all seasons, however, there was an abrupt increase in the PHg/PC ratio from an average of 0.07 ± 0.02 over the upper 150 m to 0.13 ± 0.03 between 175 m and 400 m (Table 1, Fig. 3). May was characterized by the sharpest transition and a subsurface peak in the PHg/PC ratio of small particles. Large particle PHg/PC ratios were generally lower than those measured in the small particle pool and tended to increase with increasing depth (Fig. 3). This increase in the large particle PHg/PC ratio was again almost entirely driven by a greater reduction in PC concentration over the upper 150 m across all seasons.

At 8° and 5°N, PHg/PC ratio profiles differ and did not show the same increase at 175–200 m observed at Station ALOHA. At 5°N, small particle PHg/PC ratios gradually increased from 0.02 at 5 m to 0.13 at 400 m. At 8°N, small particle PHg/PC ratios were characterized by a subsurface minimum of 0.02 fmol $nmol^{-1}$ at 50 m (Fig. 3), followed by a gradual and variable increase to 0.14 at 250 m. At depth, however, small particle PHg/PC ratios were similar to those found at Station ALOHA. Large particle PHg/PC ratios at 5°N did not change with depth, and unlike Station ALOHA, were significantly higher than the small particle ratios throughout the upper water column (t-test, $p < 0.05$). At 8°N, large particle PHg/PC ratios were much more variable, but not significantly different from those measured in small particles (Fig. 3). Ratios of MeHg/PC ranged from 0.0002 fmol $nmol^{-1}$ (25 m, 8°N, >53 µm) to 0.0029 fmol $nmol^{-1}$ (150 m, 5°N, >53 µm). Note that ratios of PC/Th are discussed in detail in Umhau et al. (2019), and seasonal and spatial changes were also largely driven by changes in PC concentrations relative to comparatively consistent ^{234}Th activities.

4.5. *Elemental particle fluxes derived using ^{234}Th:^{238}U disequilibrium*

Small and large particle PHg to ^{234}Th ratios measured at a specific depth horizon of interest were used to determine ^{234}Th derived PHg throughout the water column according to the methods described in Umhau et al. (2019). Thorium-derived PC fluxes have been previously

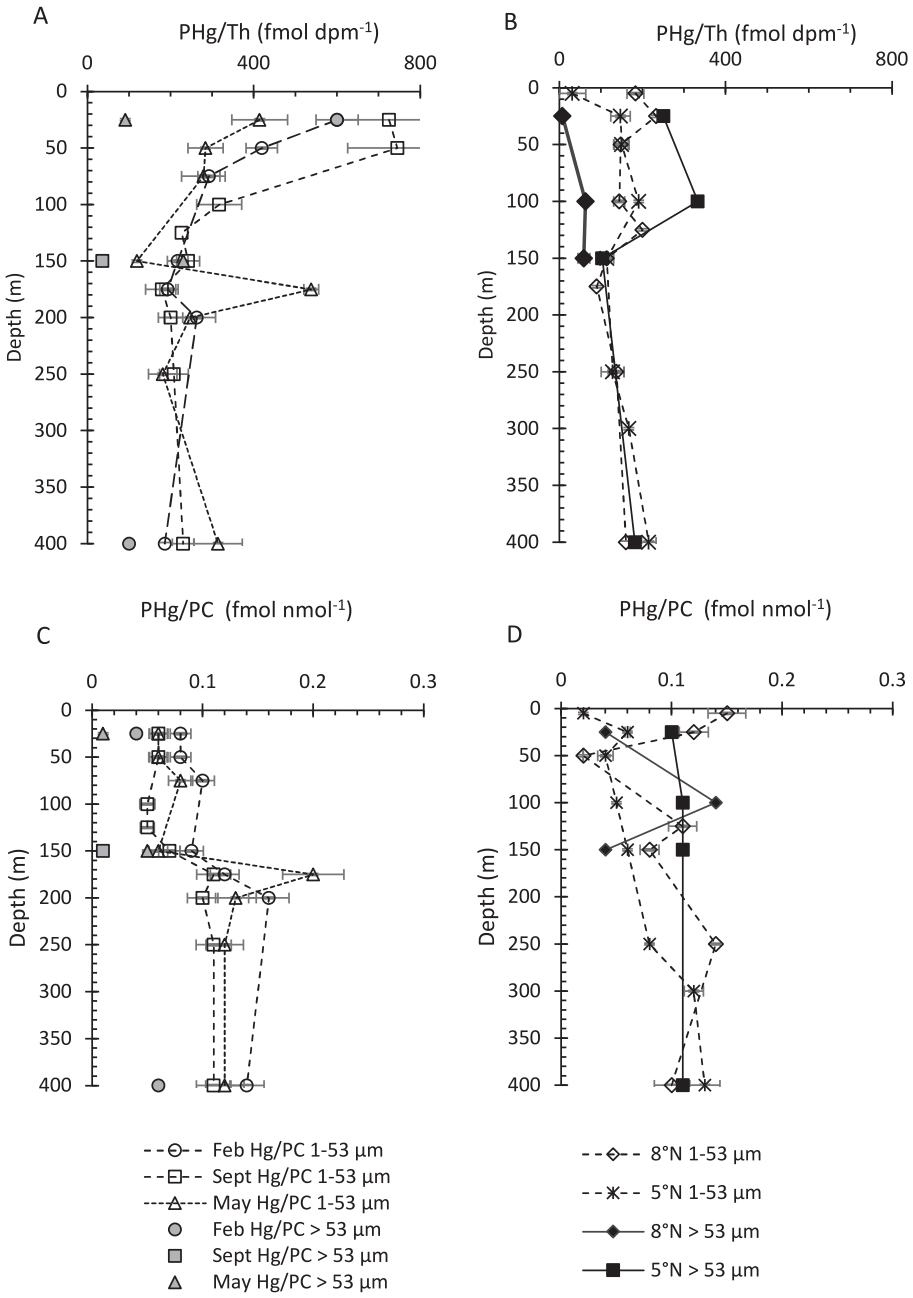

Fig. 3. Plots showing particulate mercury (PHg) to particulate thorium (Th) ratios at Station ALOHA (A) and at 5° and 8°N along 150°W (B), and PHg to particulate carbon (PC) ratios at Station ALOHA (C) and 5° and 8°N along 150°W (D) with depth in the 1–53 µm and > 53 µm size fractions.

presented in detail in Umhau et al. (2019). At Station ALOHA, PHg fluxes using small particle PHg/Th ratios ranged from below detection to 356 pmol m^{-2} day^{-1}, depending on the depth (Fig. 4). Small particle PHg fluxes in February and May were characterized by subsurface peaks just below the deep chlorophyll maximum at 150–200 m. In February, small particle PHg fluxes decreased to below detection by 400 m, while in May and September significant fluxes were still observed by 400 m. In September, small particle PHg fluxes increased throughout the water column (Fig. 4). Particulate Hg fluxes derived using large particle PHg/Th ratios are difficult to compare given the limited data (Fig. 4). Large particle PHg fluxes ranged from below detection to 160 pmol m^{-2} day^{-1}. In May, the large particle PHg flux at 150 m (160 pmol m^{-2} day^{-1}) was two times higher than the small particle PHg flux (82 pmol m^{-2} day^{-1}). Conversely in September, the large particle PHg flux at 150 m was more than six times lower than the small particle PHg derived flux. In February at 25 and 400 m (where data are available), there was no difference between small and large particle PHg fluxes. It is important to note that in February, the large particle PHg flux at 400 m was estimated using particulate ^{234}Th activity at 250 m (no data available at 400 m) and Hg concentrations measured at 400 m. This is reasonable given that large particulate ^{234}Th concentrations remained relatively constant below 150 m (see Table 1).

Along the transect stations, small particle PHg fluxes were lower throughout the water column than those measured at Station ALOHA (t-test, $p < 0.05$, $N = 43$). Small particle PHg fluxes ranged from below detection to 86 pmol m^{-2} day^{-1}, and large particle PHg fluxes ranged from below detection to 150 pmol m^{-2} day^{-1}. Small particle PHg fluxes were higher at 5°N, averaging 42 ± 13 pmol m^{-2} day^{-1} between 5 m

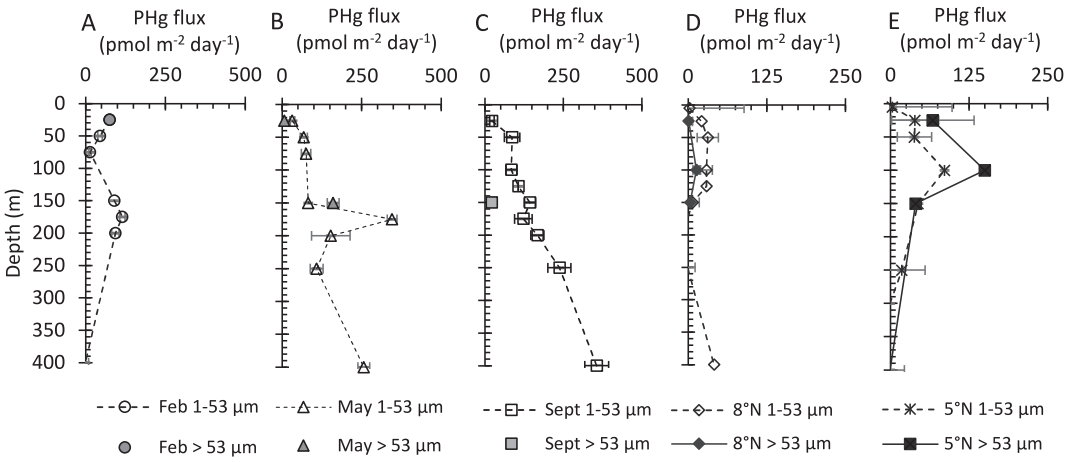

Fig. 4. Plots of particulate mercury (PHg) fluxes with depth for small (1–53 µm) and large (> 53 µm) particles derived using 238 U-234Th disequillibria and in-situ pumps. Small and large particulate Hg fluxes collected from Station ALOHA in February are shown in panel A; May data from Station ALOHA are plotted in panel B. Data collected at Station ALOHA in September are shown in panel C, and panels D and E depicts data from 8°N and 5°N respectivley along 155°W. Error bars indicate standard error and in some cases are smaller than the symbol.

and 150 m before decreasing to below detection at 300 m. At 8°N, small particle PHg fluxes were lower, averaging 20 ± 12 pmol m^{-2} day^{-1} over the upper 150 m. Below 150 m, fluxes again decreased to below detection, before increasing slightly at 400 m (Fig. 4). At 8°N, the large particle PHg flux at 150 m was 3 pmol m^{-2} day^{-1}, compared to 40 pmol m^{-2} day^{-1} at 5°N (Table 2). MeHg fluxes on small and large particles were two orders of magnitude lower than total Hg fluxes where data are available (Table 3), ranging from below detection (multiple depths) to 1.09 ± 0.57 pmol m^{-2} day^{-1} (150 m, 5°N).

5. Discussion

Sinking particles are a major pathway for transporting material from the surface ocean to the deeper waters of the mesopelagic and play a fundamental role in the biogeochemical cycling of many trace elements, including Hg (Blum et al., 2020; Hannides et al., 2015; Haskell et al., 2013; Honjo et al., 2008; Lamborg et al., 2016; Siegel et al., 2016; Tesan Onrubia et al., 2020). These sinking particles also serve as a critical food source, transferring contaminants into the food web where they may accumulate and reach high enough concentrations in commercial seafood to be a concern for public health (Blum et al., 2013; Buesseler et al., 2006; Motta et al., 2019; Siegel et al., 2014). While inorganic mercury and MeHg are both particle reactive, MeHg bioaccumulates in organism tissues (Blum et al., 2013; Lamborg et al., 2014). Blum et al. (2013) further suggests that sinking particles play an important role in introducing MeHg into the subsurface foodweb, and Choy et al. (2009 and references therein) found that the majority of Hg in fish is in the form of MeHg, which was likely introduced into the food web in the form of small particles containing MeHg (also see Sunderland et al., 2009). Tesán Onrubia et al. (2020) hypothesized that Hg particle fluxes contributed to MeHg production in the Arctic, and Motta et al. (2019) found that Hg isotopic compositions indicated that MeHg bioaccumulation is tightly linked to zooplankton mediated particle cycling. Furthermore, Motta et al. (2022) hypothesize that the particulate MeHg that enters the food web is methylated in situ from PHg.

5.1. Thorium derived particle export

By using ^{234}Th:^{238}U disequilibria measurements to estimate flux, relatively high-resolution vertical distributions of particle export and remineralization rates can be obtained (Buesseler et al., 2009). Temporal resolution is limited to the half-life of the ^{234}Th. As such, the fluxes presented here represent integrated averages over the ~35 days prior to sample collection and are less sensitive to short term phenomena (Umhau et al., 2019).

At Station ALOHA, previous measurements of total ^{234}Th:^{238}U disequilibria profiles, ^{234}Th fluxes, and small and large particulate ^{234}Th activities (Benitez-Nelson et al., 2001a; Buesseler and Boyd, 2009) were similar to those found here and described in Umhau et al. (2019). Flux errors were relatively high because the small disequilibria measured between ^{238}U and ^{234}Th activity resulted in high error propagation which is characteristic of oligotrophic sites (Buesseler et al., 2009). Because only a single thorium profile was used to calculate fluxes, and errors only include measurement uncertainties, estimated flux errors should be considered minimum estimates (Umhau et al., 2019). Despite associated large uncertainties, the range of ^{234}Th fluxes measured at 150 m (414–692 dpm m^{-2} day^{-1}) at Station ALOHA in this study were similar to those reported in previous work (377 dpm m^{-2} day^{-1} Buesseler and Boyd, 2009) and 765 dpm m^{-2} day^{-1} (Benitez-Nelson et al., 2001a; Benitez-Nelson et al., 2001b)).

There is limited information regarding ^{234}Th derived particle fluxes at 5°- 17.5°N. ^{234}Th:^{238}U disequilibria profiles, ^{234}Th fluxes, and small and large particulate ^{234}Th activities used for this study (Umhau et al., 2019) were within the range, albeit on the lower end, of values previously reported in the central Pacific (Black et al., 2018; Dunne et al., 2000; Murray et al., 2005). Fluxes were lower than those measured in February at Station ALOHA, with fluxes below detection by 125 m at 8°N and 250 m at 5°N. Higher fluxes at 5°N compared to 8°N were associated with higher primary productivity closer to the equator. Low fluxes overall were likely due to the El Niño conditions that reduced upwelling and biological production at the time of sampling (Hernes et al., 2001; Landry et al., 1997; Umhau et al., 2019).

5.2. Particulate hg and MeHg concentrations

Mercury is primarily deposited to the open ocean from the atmosphere as inorganic Hg via episodic rain events, although dry deposition does occur (Fitzgerald et al., 2007; Fitzgerald and Lamborg, 2003; Motta et al., 2019). Once gaseous Hg is released into the atmosphere from industrial activities, it rapidly spreads far from its source due to its high volatility, allowing it to be deposited in remote areas such as the central gyres (Fitzgerald et al., 2007; Fitzgerald and Lamborg, 2003; Lamborg et al., 2014) after atmospheric oxidation to Hg(II). Once deposited, oxidized Hg may then adsorb onto particles and/or be transformed into different forms via photodegradation or biological consumption and repackaging (Fitzgerald et al., 2007; Fitzgerald and Lamborg, 2003; Motta et al., 2019).

Concentrations of PHg on small particles at Station ALOHA varied

little with season and were not significantly different from those measured further south along the transect (*t*-test $p > 0.05$). While seasonal changes in atmospheric Hg deposition to this region may be possible (Chen et al., 2014), there are no measurements that suggest this is the case, inclusive of this study.

Using isotopic signatures of Hg collected concurrently, Motta et al. (2019, 2022) suggested that dissolved Hg concentrations in the surface waters at Station ALOHA, and consequently, particulate Hg concentrations, originated from wet and dry precipitation. It is likely that lower surface Hg concentrations (e.g., at 5°N) in this study were due to higher evasion rates from prevailing winds (Munson et al., 2015). Additionally, at 5°N, PHg concentrations are likely lower at 5 m compared to 25 m due to photoreduction of Hg(II) to Hg(0) and subsequent evasion of Hg(0) from surface waters into the atmosphere (Luo et al., 2020; Motta et al., 2022). Deeper in the water column, our results showed PHg concentrations on small particles at 150 m remained relatively constant with latitude (25 ± 9 fmol L^{-1}). Munson et al. (2015) measured similar PHg concentrations on particles in the 1–51 μm size fraction, ranging from 0.01 to 0.05 pmol L^{-1} (10–50 fmol L^{-1}) in this region.

Compared to small particles, concentrations of PHg on large particles were an order of magnitude lower. In samples taken concurrently, Motta et al. (2019, 2022) found that in addition to direct atmospheric PHg deposition, PHg was likely produced from adsorption of dissolved Hg onto particles. This process produces higher PHg concentrations in the smaller size fraction due to the greater surface area to volume ratio on small particles that facilitates greater adsorption of Hg compared to large particles (Fig. 4). It is important to note that there are other, likely biological factors at work that also influence particle concentration and composition (Lamborg et al., 2014).

MeHg concentrations measured on small particles in this study were at the lower end of MeHg concentrations found by Munson et al. (2015), which ranged from 0.1 to 3.1 fmol L^{-1}. Where data were available, MeHg concentrations on particles in both size fractions were higher deeper in the water column compared to surface concentrations. MeHg as a percent of PHg was also up to seven times higher (0.5 to 4%) at deeper depths relative to near-surface values where measurements were made (e.g., 8°N, 100 m verus 25 m). These results are consistent with the hypothesis that MeHg in pelagic environments is produced in situ below the euphotic zone (Blum et al., 2012, 2020; Motta et al., 2019, 2022; Munson et al., 2015). Nonetheless, MeHg as a percent of PHg remains a small percentage of PHg overall and is at the lower end of that measured in other studies (2–10%, eg. Hammerschmidt et al., 2013 and references therein).

5.3. PHg/C ratios

In order to better understand the potential role of biological productivity and carbon cycling on PHg concentrations and particle export, we examined the ratio of PHg/PC on small particles, similar to the approach of Munson et al., 2015. Note the limited large particle data did not allow for discernable PHg/PC trends to be observed. Overall, there was little seasonal variation in the small particle PHg/PC ratio throughout the water column at Station ALOHA (Fig. 3C). Vertically, however, small particle PHg/PC ratios showed a sharp increase, by a factor of two to three, between 150 and 200 m (Fig. 3C). This increase is especially evident in May, when there is a concomitant sharp increase in PHg/Th and a smaller, but significant increase in PC/Th (Fig. 3A, and see Fig. 4 in Umhau et al., 2019). The increase in PHg/PC indicates a narrow depth horizon in which PC remineralization occurs relative to PHg and coincides with a transition zone in particle degradation and microbial communities: microbially mediated particle hydrolysis is apparent at this horizon, based on the increase in $\delta^{15}N$ values of source amino acids (Hannides et al., 2013; Romero-Romero et al., 2020), and the microbial community shifts to one with larger genomes and increasing cellular nitrogen content (Mende et al., 2017).

At the Equatorial stations, trends in PHg/PC ratios are less clear, likely due to the low atmospheric deposition of Hg and biological production occurring at this site during the time of sampling (Hernes et al., 2001; Landry et al., 1997; Umhau et al., 2019). Unlike at Station ALOHA, PHg/PC ratios down the water column did not exhibit an abrupt increase with greater depth. Instead, PHg/PC ratios, although variable, gradually increased from the surface to 400 m at 5°N and between 50 and 250 m at 8°N (Fig. 3D). Similar to Station ALOHA, however, the relative increase in PHg/PC at the transect stations are likely due to preferential remineralization of PC and release to the dissolved phase compared to PHg (Munson et al., 2015; Sun et al., 2020). We hypothesize that at 8°N there was a decrease in PHg/PC from the surface to 50 m due to intense particle remineralization that masked subtle changes in particle composition, as suggested by Umhau et al. (2019). For comparison, Munson et al. (2015) measured PHg/PC ratios in sediment trap-collected particles at 60, 150 and 500 m. Ratios were similar to those measured in the small and large particles ratios and ranged from 0.01 to 0.08. Note that ratios were three to four times higher at 150 m relative to 60 m at 8°N and at the equator (Munson et al., 2015), whereas PHg/PC ratios experienced a similar increase in small particles only at 5°N.

5.4. PHg/Th ratios

The ratio of an element to ^{234}Th on particles is critical for estimating sinking particle fluxes using ^{234}Th across a specific depth horizon (Buesseler et al., 2006). This ratio changes based on the environment and can be affected by surface area to volume ratios, bacterial reworking, adsorption, and other biological, chemical and physical properties of the particles in question (Buesseler et al., 2006; Lam et al., 2015). Therefore, for the calculation of fluxes, it is important to apply the element:^{234}Th ratio found at a specific depth of interest.

In seawater the dissolution constant, K_d, of Th is similar to that of Hg (Lamborg et al., 2016), which means the PHg/Th ratio should vary little if only influenced by equilibrium chemistry. Similar to particulate Th, PHg undergoes regenerative scavenging (Bowman et al., 2020), meaning that PHg reversion to dissolved Hg is not governed so much by desorption, but instead by remineralization of the entire particle to release PHg back into the dissolved phase. Unlike particulate Th, however, a secondary biologically mediated pathway also occurs for PHg (Cui et al., 2021).

At Station ALOHA, small particle PHg/Th ratios generally decreased rapidly from the surface to 150 m driven by changes in PHg (Fig. 3A). In contrast, at the transect stations, small and large particulate PHg/Th ratios from the Equatorial stations, while also driven by Hg concentrations, had much smaller to no changes with depth. PHg/Th ratios were highest between 25 and 100 m and at 400 m at 5°N, and between 5 and 125 m at 8°N. The preferential removal of PHg relative to particulate Th is consistent with strong microbially mediated reworking and remineralization at Station ALOHA (Cui et al., 2021). These biologically mediated processes are much less dominant at the Equator, again consistent with the lower biological productivity occurring at this site during the time of sampling. Although limited, PHg/Th ratios on large particles are the same or lower than those measured at the same depths in small particles.

At Station ALOHA in May at 175 m, there was an abrupt increase in PHg/Th that aligns with the sharp increase in PHg/PC, suggesting preferential remineralization of PC or incorporation of Hg into particles at this depth. This also observed at 200 m in February, but to a much lesser extent. Although there were no abrupt increases in PHg/Th or PHg/PC at the transect stations, the highest PHg/Th ratios align with the depth range where PHg/PC ratios gradually increased (Fig. 3). Variations in PHg and elemental ratios (PHg/Th and PHg/PC) within the euphotic zone coincide with a transition zone in particle degradation and a change in microbial community (Mende et al., 2017). Motta et al. (2022) also identified increased microbial reworking of Hg within small particles between 100 and 150 m at the transect stations that likely stimulated MeHg production and subsequent uptake. There is no isotope

data below 150 m from Station ALOHA to fingerprint the abrupt PHg/Th and PHg/PC increase below 150 m, but we suspect similar processes at work.

5.5. PHg fluxes

Quantifying the magnitude of PHg sinking fluxes is a crucial part of understanding Hg cycling and the depths at which Hg may be introduced into the food web (Munson et al., 2015). This study provides some of the first measurements of sinking PHg and MeHg fluxes in the NPSG using in situ pumps and how those fluxes change with water depth and season. Due to the paucity of large particle PHg measurements, we focus the rest of this discussion on small particle-derived PHg fluxes, noting that when available, small and large particle PHg/Th derived PHg fluxes were similar (Fig. 4).

Station ALOHA is subject to summer export pulse, when particle fluxes are higher than the rest of the year and fluxes increase with depth in the water column (Umhau et al., 2019 and references therein). At Station ALOHA, while euphotic zone PHg concentrations in the 1–53 μm size fraction were less seasonally variable than those seen in PC (Umhau et al., 2019), PHg fluxes on small particles generally increased from February to September. Subsurface maxima in February and May export fluxes occurred at 175 m, at or just below the depth of maximum fluxes in PC export at 175 and 150 m, respectively. The general increase in PHg flux throughout the water column in September is associated with larger *Trichodesmium* spp. in the phytoplankton assemblage that aggregate and sweep the upper column of particles as material sinks through the water column (Gosnell and Mason, 2015; Pasulka et al., 2013).

In September, PHg fluxes continue to increase to 400 m, reaching fluxes that are more than double that measured at 150 m. These relative changes in PHg flux are higher than that measured for fluxes of PC (Umhau et al., 2019). For example, the PC flux increases by twofold from the surface to 400 m versus a fourfold increase in PHg. While changes in PC flux are dominated by biological processes, Hg fluxes are also fundamentally influenced by scavenging and reduction/oxidation reactions (Fitzgerald et al., 2007; Munson et al., 2015). Munson et al. (2015) also found that PHg was preferentially transported to depth compared to PC.

High PHg fluxes below 150 m in May and September are further consistent with the "regenerative scavenging" model of Hg particle-dissolution dynamics (Lamborg et al., 2016; Siegel et al., 2014) and help to explain the high Hg concentrations measured in pelagic fish that forage in this depth range (Choy et al., 2009; Hannides et al., 2020; Romero-Romero et al., 2020.

Small particle PHg fluxes measured at 150 m at Station ALOHA were generally much higher (82–143 pmol m^{-2} d^{-1}, Table 1) than the sediment trap fluxes reported by Munson et al. (2015) (30 ± 34 pmol m^{-2} d^{-1}) at 17°N, but similar to fluxes reported at the equator (123 ± 23 pmol m^{-2} d^{-1}). Tesan Onrubia et al. (2020) used ^{238}U: ^{234}Th disequilibria to calculate small particle PHg fluxes in the Arctic and reported average fluxes of 95 ± 195 pmol m^{-2} d^{-1} at 100 m in the central Arctic under ice cover, and much higher fluxes on the outer shelf (635 ± 480 pmol m^{-2} d^{-1}) where primary production rates were higher.

PHg fluxes at the transect stations were much lower than those measured at Station ALOHA and reflected lower particle loads and lower biological activity at the time of sampling. Umhau et al. (2019) found that concurrent PC export fluxes were low at 5°N and 8°N compared to May and September at Station ALOHA and attenuated quickly due to El Niño conditions that suppressed the typical equatorial upwelling and decreased surface primary production. Munson et al. (2015) also reported low mass flux in this region in 2011, a strong La Niña period. It is likely that reduced export flux in both particle size fractions was the main driver of PHg flux attenuation at the transect stations (Umhau et al., 2019) rather than preferential removal of particulate Hg. The constant Hg/Th ratio throughout the water column supports this hypothesis (Fig. 3). The MeHg fluxes reported in this study are similar to those reported in Munson et al. (2015) at 8°N and 0°N using sediment traps.

5.6. Particulate hg cycling in the North Pacific Ocean

Increased PHg concentrations and higher elemental ratios (PHg/Th and PHg/PC) within the euphotic zone at the transect stations and at depth at Station ALOHA coincide with increased microbial activity according to δ^{15}NSrc-AA (Romero-Romero et al., 2020) and Hg stable isotope data (Motta et al., 2022). The relative increase in δ^{15}NSrc-AA at Station ALOHA and transect stations between 100 m and 250 m indicates heightened microbial degradation within this depth range, affecting small particles with a higher surface area to volume, to a greater extent than large particles. At the Equator, PHg fluxes were highest between 25 and 150 m. At Station ALOHA, the relative changes in PHg fluxes were, in some cases, higher than those observed in PC fluxes in the upper 400 m (Fig. 4; refer to Station ALOHA September PHg fluxes). These findings align with Hg stable isotope data (Motta et al., 2019), indicating increased Hg methylation that mediates Hg bioaccumulation into particles.

Collectively, our findings suggest that microbial consortia at varying depths not only influence PHg and PC concentrations throughout the water column but also exhibit regional variability, consistent with observed differences in PHg/PC ratios across latitudes (Bianchi et al., 2018; Blum et al., 2013), and potentially leading to changes in Hg speciation and flux to depth. Increased microbial activity can stimulate the formation of MeHg, which is available for uptake and bioaccumulation. Enhanced Hg methylation (Lamborg et al., 2016) and elevated MeHg concentrations below 150 m, as measured by Munson et al. (2015) and confirmed in particles at depth in this study (Table 3), support this observation. The increased proportions of MeHg in the upper mesopelagic represent an additional mechanism for subsurface uptake and bioaccumulation of Hg into particles via microbial activity.

Recent hypotheses, such as those presented by Heimbürger et al. (2010) and Sun et al. (2014), suggest that increased PHg flux may be facilitated by MeHg bioaccumulation during feeding. This aligns with the findings of Romero-Romero et al. (2020), who argued that microbial reworking of small particles was more significant than zooplankton grazing in September at Station ALOHA. Interestingly, where data was available, MeHg fluxes did not follow the same trends in PHg fluxes, indicating possible preferential bioaccumulation, remineralization, or demethylation of particulate MeHg.

Motta et al. (2022) proposed that MeHg production is most efficient in the upper 400 m, and below this depth, demethylation, among other processes, outcompetes Hg methylation. This may explain why the observed patterns in PHg/PC and PHg/Th are not evident at greater depths and are restricted to a narrow zone within the upper water column. Although the MeHg fraction in both large and small particles was minimal, potentially due to uptake and bioaccumulation, changes in total PHg and elemental ratios also likely reflect the impact of microbial mediated MeHg production within the euphotic zone and upper mesopelagic. While the PHg and elemental ratios could also be altered by metabolite production from elevated microbial activity via Hg complexation, the Hg stable isotope particulate results indicate this was not a predominate pathway below upper euphotic zone (Motta et al., 2019; Motta et al., 2022). Our results in conjunction with the Hg stable isotope data from Station ALOHA and the transect stations support the growing evidence that Hg methylation likely occurs below the surface mixed layer (Blum et al., 2013; Motta et al., 2019, 2022) and is a crucial source of Hg for the marine food web, necessitating consideration in models exploring marine Hg biogeochemistry.

6. Conclusions

The disequilibrium between ^{238}U and ^{234}Th was used to measure PHg fluxes throughout the water column during the winter, late spring/

early summer and late summer at Station ALOHA in the NPSG, and across a latitudinal gradient from 5°N -17.5°N along 155°W. At Station ALOHA, PHg/PC and PHg/Th ratios, supported by Hg and amino acid isotopic data, indicate that PC is preferentially remineralized relative to PHg and that PHg is preferentially remineralized relative to PTh due to microbially mediated hydrolysis. The abrupt increase in PHg relative to PC and PTh at depth appears to be mediated, at least in part, by microbially mediated methylation. Similar processes are likely occurring at the equator, with lower biological activity and particle fluxes obscuring depth trends. At Station ALOHA, PHg fluxes displayed a seasonal trend, highest in September and lowest in February, due to increased summer particle production followed by bioaccumulation. PHg fluxes at Station ALOHA are high, and subsurface fluxes coupled with possible in situ MeHg production may explain the high Hg concentrations measured in pelagic fish. Combined, this work argues that subsurface Hg cycling may be critical for understanding Hg bioaccumulation in marine systems. Fluxes of Hg on large particles are some of the first ever published and indicate that particle size class should be accounted for when trying to characterize Hg biogeochemical cycling, although large particle PHg is a small fraction of the PHg particle pool. Our results contribute significantly to the understanding of Hg transport to the ocean interior. This information is crucial for estimating the bioavailability of Hg for methylation and its uptake by marine food webs. Consequently, our findings should inform oceanic Hg models, which are necessary for projecting MeHg changes in food webs in a changing climate (Schartup et al. (2019); Zhang et al., 2021).

CRediT authorship contribution statement

Blaire P. Umhau: Writing – review & editing, Writing – original draft, Methodology, Formal analysis, Data curation. **Laura C. Motta:** Writing – review & editing, Writing – original draft, Methodology, Investigation, Formal analysis. **Joel D. Blum:** Writing – review & editing, Writing – original draft, Funding acquisition, Conceptualization. **Hilary G. Close:** Writing – review & editing, Writing – original draft, Methodology, Formal analysis. **Jeffrey C. Drazen:** Writing – review & editing, Writing – original draft, Investigation, Conceptualization. **Brian N. Popp:** Writing – review & editing, Writing – original draft, Project administration, Investigation, Funding acquisition, Conceptualization. **Claudia R. Benitez-Nelson:** Writing – review & editing, Writing – original draft, Supervision, Project administration, Investigation, Funding acquisition, Formal analysis, Data curation, Conceptualization.

Data availability

Data will be made available on request.

Acknowledgments

We would like to thank the captain and crew of the R/V *Kilo Moana*, Justin Miyano, Meryssa Piper, Kalina Grabb, Natalie Wallsgrove, Kelly McCabe, Daniel Wade and Marc Humphries for their assistance with pump deployment and sample collection. This work was funded by National Science Foundation grant OCE 1433313, and BU was supported by a University of South Carolina Presidential Fellowship. We would like to also thank two anonymous reviewers for their insightful comments and constructive suggestions. This is SOEST contribution number 11817.

References

Alonso-Gonzalez, I.J., Aristegui, J., Lee, C., Sanchez-Vidal, A., Calafat, A., Fabres, J., Sangra, P., Masque, P., Hernandez-Guerra, A., Benitez-Barrios, V., 2010. Role of slowly settling particles in the ocean carbon cycle. Geophys. Res. Lett. https://doi.org/10.1029/2010GL043827.

Anderson, R.F., 2020. GEOTRACES: accelerating research on the marine biogeochemical cycles of trace elements and their isotopes. Annu. Rev. Mar. Sci. 12, 49–85 doi: https://doi-org.library.proxy.mbl.edu/10.1146/annurev-marine-010318-095123.

Bacon, M.P., Cochran, J.K., Hirschberg, D., Hammar, T.R., Fleer, A.P., 1996. Export flux of carbon at the equator during the EqPac time-series cruises estimated from 234Th measurements. Deep. Res. Part II Top. Stud. Oceanogr. 43, 1133–1153. https://doi.org/10.1016/0967-0645(96)00016-1.

Benitez-Nelson, C.R., Buesseler, K.O., Karl, D.M., Andrews, J., 2001a. A time-series study of particulate matter export in the North Pacific subtropical gyre based on 234 Th : 238 U disequilibrium. Deep Sea Res. I 48, 2595–2611.

Benitez-Nelson, C.R., Buesseler, K.O., van der Loeff, M.R., Andrews, J., Ball, L., Crossin, G., Charette, M.A., 2001b. Testing a new small-volume technique for determining 234 Th in seawater. J. Radioanal. Nucl. Chem. 248, 795–799.

Bianchi, D., Weber, T.S., Kiko, R., Deutsch, C., 2018. Global niche of marine anaerobic metabolisms expanded by particle microenvironments. Nat. Geosci. 11, 263–268. https://doi.org/10.1038/s41561-018-0081-0.

Biswas, A., Blum, J.D., Bergquist, B.A., Keeler, G.J., Xie, Z., 2008. Natural mercury isotope variation in coal deposits and organic soils. Environ. Sci. Technol. 42, 8303–8309 doi:10.1021/es801444b.

Black, F.J., Poulin, B.A., Flegal, A.R., 2012. Factors controlling the abiotic photodegradation of monomethylmercury in surface waters. Geochim. Cosmochim. Acta 84, 492–507. https://doi.org/10.1016/j.gca.2012.01.019.

Black, E.E., Buesseler, K.O., Pike, S.M., Lam, P.J., 2018. 234Th as a tracer of particulate export and remineralization in the southeastern tropical Pacific. Mar. Chem. 201, 35–50. https://doi.org/10.1016/j.marchem.2017.06.009.

Blum, J.D., Popp, B.N., Drazen, J.C., Anela Choy, C., Johnson, M.W., 2013. Methylmercury production below the mixed layer in the North Pacific Ocean. Nat. Geosci. 6, 879–884. https://doi.org/10.1038/ngeo1918.

Blum, J.D., Drazen, J.C., Johnson, M.W., Popp, B.N., Motta, L.C., Jamieson, A.J., 2020. Mercury isotopes identify near-surface marine mercury in deep-sea trench biota. Proc. Natl. Acad. Sci. USA 117, 29292–29298. https://doi.org/10.1073/pnas.2012773117.

Böttjer, D., Dore, J.E., Karl, D.M., Letelier, R.M., Mahaffey, C., Wilson, S.T., Zehr, J., Church, M.J., 2017. Temporal variability of nitrogen fixation and particulate nitrogen export at station ALOHA. Limnol. Oceanogr. 62, 200–216. https://doi.org/10.1002/lno.10386.

Bowman, K.L., Lamborg, C.H., Agather, A.M., 2020. A global perspective on mercury cycling in the ocean. Sci. Total Environ. 710, 136166 https://doi.org/10.1016/j.scitotenv.2019.136166.

Buesseler, K.O., Boyd, P.W., 2009. Shedding light on processes that control particle export and flux attenuation in the twilight zone of the open. Limnol. Oceanogr. 54, 1210–1232.

Buesseler, K., Andrews, J.A., Hartman, M.C., Belastock, R., Chai, F., 1995. Regional estimates of the export flux of particulate organic carbon derived from thorium-234 during the JGOFS EqPac program. Deep-Sea Res. II 42, 777–804.

Buesseler, K.O., Benitez-Nelson, C., Rutgers Van Der Loeff, M., Andrews, J., Ball, L., Crossin, G., Charette, M.A., 2001. An intercomparison of small-and large-volume techniques for thorium-234 in seawater. Mar. Chem. 74, 15–28. https://doi.org/10.1016/S0304-4203(00)00092-X.

Buesseler, K.O., Benitez-nelson, C.R., Moran, S.B., Burd, A., Charette, M., Cochran, J.K., Coppola, L., Fisher, N.S., Fowler, S.W., Gardner, W.D., Guo, L.D., Gustafsson, O., Lamborg, C., Masque, P., Miquel, J.C., Passow, U., Santschi, P.H., Savoye, N., Stewart, G., Trull, T., 2006. An assessment of particulate organic carbon to thorium-234 ratios in the ocean and their impact on the application of 234 Th as a POC flux proxy. Mar. Chem. 100, 213–233. https://doi.org/10.1016/j.marchem.2005.10.013.

Buesseler, K.O., Trull, T.W., Steinberg, D.K., Silver, M.W., Siegel, D.A., Saitoh, S., Lamborg, C.H., Lam, P.J., Karl, D.M., Jiao, N.Z., Honda, M.C., Elskens, M., Dehairs, F., Brown, S.L., Boyd, P.W., Bishop, J.K.B., Bidigare, R.R., 2008. VERTIGO (VERtical transport in the Global Ocean): a study of particle sources and flux attenuation in the North Pacific. Deep. Res. II 55, 1522–1539. https://doi.org/10.1016/j.dsr2.2008.04.024.

Buesseler, K.O., Pike, S., Maiti, K., Lamborg, C.H., Siegel, D.A., Trull, T.W., 2009. Thorium-234 as a tracer of spatial, temporal and vertical variability in particle flux in the North Pacific. Deep. Res. Part I 56, 1143–1167. https://doi.org/10.1016/j.dsr.2009.04.001.

Buesseler, K.O., Boyd, P.W., Black, E.E., Siegel, D.A., 2020. Metrics that matter for assessing the ocean biological carbon pump. Proc. Natl. Acad. Sci. USA 117, 9679–9687. https://doi.org/10.1073/pnas.1918114117.

Chen, L., Wang, H.H., Liu, J.F., Tong, Y.D., Ou, L.B., Zhang, W., Hu, D., Chen, C., Wang, X.J., 2014. Intercontinental transport and deposition patterns of atmospheric mercury from anthropogenic emissions. Atmos. Chem. Phys. 10163–10176 https://doi.org/10.5194/acp-14-10163-2014.

Choy, C.A., Popp, B.N., Kaneko, J.J., Drazen, J.C., 2009. The influence of depth on mercury levels in pelagic fishes and their prey. Proc. Natl. Acad. Sci. USA 106, 13865–13869. https://doi.org/10.1073/pnas.0900711106.

Choy, C.A., Popp, B.N., Hannides, C.C.S., Drazen, J.C., 2015. Trophic structure and food resources of epipelagic and mesopelagic fishes in the north pacific subtropical gyre ecosystem inferred from nitrogen isotopic compositions. Limnol. Oceanogr. https://doi.org/10.1002/lno.10085.

Church, M.J., Lomas, M.W., Muller-karger, F., 2013. Deep-Sea research II Sea change : charting the course for biogeochemical ocean time-series research in a new millennium. Deep. Res. Part II 93, 2–15. https://doi.org/10.1016/j.dsr2.2013.01.035.

Coale, K.H., Bruland, K.W., 1985. ^{234}Th:^{238}U diseuilibria within the alifronia current. Limnol. Oceanogr. 30, 22–33.

Cossa, D., Harmelin-Vivien, M., Mellon-Duval, C., Loizeau, V., 2009. Bioamplification of methylmercury in two trophically dissimilar marine ecosystems. In: Geochimica et Cosmochimica Acta, p. A245.
Cossa, D., Rintoul, S.R., Cossa, D., Heimbu, L., Rintoul, S.R., Butler, E.C.V., Bowie, A.R., 2011. Mercury in the Southern Ocean mercury in the Southern Ocean. Geochim. Cosmochim. Acta 75, 4037–4052.
Cossa, D., Harmelin-Vivien, M., Mellon-Duval, C., Loizeau, V., Averty, B., Crochet, S., Chou, L., Cadiou, J.-F., 2012. Influences of bioavailability, trophic position, and growth on methylmercury in hakes (Merluccius merluccius) from northwestern Mediterranean and northeastern Atlantic. Environ. Sci. Technol. 46, 4885–4893 doi: 10.1021/es204269w.
Cui, X., Lamborg, C.H., Hammerschmidt, D.R., Xiang, Y., Lam, P.J., 2021. The effect of particle composition and concentration on the partitioning coefficient for mercury in three ocean basins. Front. Environ. Chem. 2 https://doi.org/10.3389/fenvc.2021.660267.
DiMento, B.P., Mason, R.P., 2017. Factors controlling the photochemical degradation of methylmercury in coastal and oceanic waters. Mar. Chem. 196, 116–125. https://doi.org/10.1016/j.marchem.2017.08.006.Factors.
Dunne, J.P., Murray, J.W., Rodier, M., Hansell, D.A., 2000. Export flux in the western and central equatorial Pacific: zonal and temporal variability. Deep Sea Res. I 47, 901–936.
Durkin, C.A., Estapa, M.L., Buesseler, K.O., 2015. Observations of carbon export by small sinking particles in the upper mesopelagic. Mar. Chem. https://doi.org/10.1016/j.marchem.2015.02.011.
Fernández-Gómez, C., Drott, A., Björn, E., Díez, S., Bayona, J.M., Tesfalidet, S., Lindfors, A., Skyllberg, U., 2013. Towards universal wavelength-specific photodegradation rate constants for methyl mercury in humic waters, exemplified by a boreal lake-wetland gradient. Environ. Sci. Technol. 47, 6279–6287. https://doi.org/10.1021/es400373s.
Fitzgerald, W.F., Lamborg, C.H., 2003. Geochemistry of mercury in the environment. Treatise on Geochemistry 9.
Fitzgerald, W.F., Lamborg, C.H., Hammerschmidt, C.R., 2007. Marine biogeochemical cycling of mercury. Chem. Rev. 107, 641–662. https://doi.org/10.1021/cr050353m.
Gloeckler, K., Choy, C.A., Hannides, C.C.S., Close, H.G., Goetze, E., Popp, B.N., Drazen, J. C., 2018. Stable isotope analysis of micronekton around Hawaii reveals suspended particles are an important nutritional source in the lower mesopelagic and upper bathypelagic zones. Limnol. Oceanogr. 63, 1168–1180. https://doi.org/10.1002/lno.10762.
Gosnell, K.J., Mason, R.P., 2015. Mercury and methylmercury incidence and bioaccumulation in plankton from the Central Pacific Ocean. Mar. Chem. 177, 772–780. https://doi.org/10.1016/j.marchem.2015.07.005.
Grabowski, E., Letelier, R.M., Laws, E.A., Karl, D.M., 2019. Coupling carbon and energy fluxes in the North Pacific subtropical gyre. Nat. Commun. 10 https://doi.org/10.1038/s41467-019-09772-z.
Hammerschmidt, C.R., Bowman, K.L., 2012. Vertical methylmercury distribution in the subtropical North Pacific Ocean. Mar. Chem. 132–133, 77–82. https://doi.org/10.1016/j.marchem.2012.02.005.
Hammerschmidt, C.R., Finiguerra, M.B., Weller, R.L., Fitzgerald, W.F., 2013. Methylmercury accumulation in plankton on the continental margin of the Northwest Atlantic Ocean. Environ. Sci. Technol. 47, 3671–3677 doi:0.1021/es3048619.
Hannides, C.C.S., Popp, B.N., Choy, C.A., Drazen, J.C., 2013. Midwater zooplankton and suspended particle dynamics in the North Pacific subtropical gyre: a stable isotope perspective. Limnol. Oceanogr. 58 (6), 1931–1946. https://doi.org/10.4319/lo.2013.58.6.1931.
Hannides, C.C.S., Drazen, J.C., Popp, B.N., 2015. Mesopelagic zooplankton metabolic demand in the North Pacific subtropical gyre. Limnol. Oceanogr. 60, 419–428. https://doi.org/10.1002/lno.10032.
Hannides, C.C.S., Popp, B.N., Close, H.G., Benitez-Nelson, C.R., Ka'apu-Lyons, C.A., Gloeckler, K., Wallsgrove, N., Umhau, B., Palmer, E., Drazen, J.C., 2020. Seasonal dynamics of midwater zooplankton and relation to particle cycling in the North Pacific subtropical gyre. Prog. Oceanogr. 1–101.
Haskell, W.Z., Berelson, W.M., Hammond, D.E., Capone, D.G., 2013. Particle sinking dynamics and POC fluxes in the eastern tropical South Pacific based on 234Th budgets and sediment trap deployments. Deep. Res. Part I Oceanogr. Res. Pap. 81, 1–13. https://doi.org/10.1016/j.dsr.2013.07.001.
Heimbürger, L.E., Cossa, D., Marty, J.C., Migon, C., Averty, B., Dufour, A., Ras, J., 2010. Methyl mercury distributions in relation to the presence of nano- and picophytoplankton in an oceanic water column (Ligurian Sea, North-Western Mediterranean). Geochim. Cosmochim. Acta 74, 5549–5559. https://doi.org/10.1016/j.gca.2010.06.036.
Hernes, P.J., Peterson, M.L., Murray, J.W., Wakeham, S.G., Lee, C., Hedges, J.I., 2001. Particulate carbon and nitrogen fluxes and compositions in the central equatorial Pacific. Deep Sea Res Part I Oceanogr. Res. Pap. 48, 1999–2023. https://doi.org/10.1016/S0967-0637(00)00115-1.
Honjo, S., Manganini, S.J., Krishfield, R.A., Francois, R., 2008. Particulate organic carbon fluxes to the ocean interior and factors controlling the biological pump: a synthesis of global sediment trap programs since 1983. Prog. Oceanogr. 76, 217–285. https://doi.org/10.1016/j.pocean.2007.11.003.
Horowitz, H.M., Jacob, D.J., Amos, H.M., Streets, D.G., Sunderland, E.M., 2014. Historical mercury releases from commercial products: global environmental implications. Environ. Sci. Technol. 48, 10242–10250. https://doi.org/10.1021/es501337j.
Jeremiason, J.D., Portner, J.C., Aiken, G.R., Hiranaka, A.J., Dvorak, M.T., Tran, K.T., Latch, D.E., 2014. Photoreduction of hg(II) and Photodemethylation of Methylmercury: The Key Role of Thiol Sites on Dissolved Organic Matter. Environ. Sci. Process. Impacts. https://doi.org/10.4135/9781446247501.n1321
Karl, D.M., Lukas, R., 1996. The Hawaii Ocean time-series (HOT) program: background, rationale and field implementation. Deep Sea Res Part II Top. Stud. Oceanogr. 43, 129–156. https://doi.org/10.1016/0967-0645(96)00005-7.
Karl, D.M., Church, M.J., Dore, J.E., Letelier, R.M., Mahaffey, C., 2012. Predictable and efficient carbon sequestration in the North Pacific Ocean supported by symbiotic nitrogen fixation. Proc. Natl. Acad. Sci. USA 109, 1842–1849. https://doi.org/10.1073/pnas.1120312109.
Kavanaugh, M.T., Church, M.J., Davis, C.O., Karl, D.M., Letelier, R.M., Doney, S.C., 2018. ALOHA from the edge: reconciling three decades of in situ eulerian observations and geographic variability in the North Pacific subtropical gyre. Front. Mar. Sci. 5, 1–14. https://doi.org/10.3389/fmars.2018.00130.
Kennedy, P., Kennedy, H., Papadimitriou, S., 2005. The effect of acidification on the determination of organic carbon, total nitrogen and their stable isotopic composition in algae and marine sediment. Rapid Commun. Mass Spectrom. 19, 1063–1068. https://doi.org/10.1002/rcm.1889.
Kiko, R., Biastoch, A., Brandt, P., et al., 2017. Biological and physical influences on marine snowfall at the equator. Nat. Geosci. 10, 852–858 doi.org/10.1038/ngeo3042.
Lam, P.J., Ohnemus, D.C., Auro, M.E., 2015. Size-fractionated major particle composition and concentrations from the US GEOTRACES North Atlantic zonal transect. Deep. Res. Part II Top. Stud. Oceanogr. 116, 303–320. https://doi.org/10.1016/j.dsr2.2014.11.020.
Lamborg, C., Bowman, K., Hammerschmidt, C., Gilmour, C., Munson, K., Selin, N., Tseng, C.-M., 2014a. Mercury in the Anthropocene Ocean. Oceanography 27, 76–87. https://doi.org/10.5670/oceanog.2014.11.
Lamborg, C., Hammerschmidt, C., Bowman, K., et al., 2014b. A global ocean inventory of anthropogenic mercury based on water column measurements. Nature 512, 65–68 doi.org/10.1038/nature13563.
Lamborg, C.H., Hammerschmidt, C.R., Bowman, K.L., 2016. An examination of the role of particles in oceanic mercury cycling. Philos. Trans. R. Soc. A 374.
Landry, M.R., Barber, R.T., Bidare, R.R., Chai, F., Coale, K.H., Dam, H.G., Lewis, M.R., Lindley, S.T., McCarthy, J.J., Roman, M.R., Stoecker, D.K., Verity, P.G., White, J.R., 1997. Iron and grazing constraints on primary production in the central equatorial Pacific: an EqPac synthesis. Limnol. Oceanogr. 42, 405–418. https://doi.org/10.4319/lo.1997.42.3.0405.
Laurier, F.J.G., Mason, R.P., Gill, G.A., Whalin, L., 2004. Mercury distributions in the North Pacific Ocean - 20 years of observations. Mar. Chem. 90, 3–19. https://doi.org/10.1016/j.marchem.2004.02.025.
Luo, H., Cheng, Q., Pan, X., 2020. Photochemical behaviors of mercury (hg) species in aquatic systems: a systematic review on reaction process, mechanism, and influencing factor. Sci. Total Environ. 270 https://doi.org/10.1016/j.scitotenv.2020.137540.
Maiti, K., Nelson, C.R.B., Buesseler, K.O., 2010. Insights into particle formation and remineralization using the short - lived radionuclide, Thoruim - 234. Geophys. Res. Lett. 37, 2–7. https://doi.org/10.1029/2010GL044063.
Mason, R.P., Fitzgerald, W.F., 1993. The distribution and biogeochemical cycling of mercury in the equatorial Pacific Ocean. Deep. Res. Part I 40, 1897–1924. https://doi.org/10.1016/0967-0637(93)90037-4.
Mason, R.P., Sullivan, K.A., 1999. The distribution and speciation of mercury in the south and equatorial Atlantic. Deep Res. Part II Top. Stud. Oceanogr. 46, 937–956. https://doi.org/10.1016/S0967-0645(99)00010-7.
Mende, D.R., Bryant, J.A., Aylward, F.O., Eppley, J.M., Nielsen, T., Karl, D.M., Delong, E. F., 2017. Environmental drivers of a microbial genomic transition zone in the ocean's interior. Nat. Microbiol. 2, 1367–1373. https://doi.org/10.1038/s41564-017-0008-3.
Motta, L.C., Blum, J.D., Johnson, M.W., Umhau, B.P., Popp, B.N., Washburn, S.J., Drazen, J.C., Benitez-Nelson, C.R., Hannides, C.S., Close, H.G., Lamborg, C.H., 2019. Mercury cycling in the North Pacific subtropical gyre as revealed by mercury stable isotope ratios global biogeochemical cycles. Glob. Biogeochem. Cycles 33, 777–794. https://doi.org/10.1029/2018GB006057.
Motta, L.C., Blum, J.D., Popp, B.N., Umhau, B.P., Benitez-Nelson, C.R., Washburn, S.J., Drazen, J., 2022. Mercury isotopic evidence for the importance of particles as a source of mercury to marine organisms. P. Natl. Acad. Sci. 119 (44).
Munson, K.M., Lamborg, C., Swarr, G.J., Saito, M.A., 2015. Mercury species concentrations and fluxes in the central tropical Pacific Ocean. Glob. Biogeochem. Cycles 29, 656–676. https://doi.org/10.1002/2015GB005120.Received.
Murray, J.W., Paul, B., Dunne, J.P., Chapin, T., 2005. 234Th,210Pb,210Po and stable Pb in the central equatorial Pacific: tracers for particle cycling. Deep. Res. Part I Oceanogr. Res. Pap. 52, 2109–2139. https://doi.org/10.1016/j.dsr.2005.06.016.
Owens, S.A., Buesseler, K.O., Sims, K.W.W., 2011. Re-evaluating the 238 U-salinity relationship in seawater : implications for the U – 234 Th disequilibrium method. Mar. Chem. 127, 31–39. https://doi.org/10.1016/j.marchem.2011.07.005.
Owens, S.A., Pike, S., Buesseler, K.O., 2015. Thorium-234 as a tracer of particle dynamics and upper ocean export in the Atlantic Ocean. Deep Sea Res Part II Top. Stud. Oceanogr. 116, 42–59. https://doi.org/10.1016/j.dsr2.2014.11.010.
Pasulka, A.L., Landry, M.R., Taniguchi, D.A.A., Taylor, A.G., Church, M.J., 2013. Temporal dynamics of phytoplankton and heterotrophic protists at station ALOHA. Deep. Res. Part II Top. Stud. Oceanogr. 93, 44–57. https://doi.org/10.1016/j.dsr2.2013.01.007.
Pike, S.M., Buesseler, K.O., Andrews, J., Savoye, N., 2005. Quantification of 234 Th recovery in small volume sea water samples by inductively coupled plasma-mass spectrometry. J. Radioanal. Nucl. Chem. 263, 355–360.
Puigcorbé, V., Benitez-nelson, C.R., Masqué, P., Verdeny, E., White, A.E., Popp, B.N., Prahl, F.G., Lam, P.J., 2015. Small phytoplankton drive high summertime carbon

and nutrient export in the Gulf of California and eastern tropical North Pacific. Glob. Biogeochem. Cycles 1309–1332. https://doi.org/10.1002/2015GB005134.
Richardson, T.L., Jackson, G.A., 2007. Small phytoplankton and carbon export from the Surface Ocean. Science (80-.) 838–840. https://doi.org/10.1126/science.1133471.
Romero-Romero, S., Ka'apu-Lyons, C.A., Umhau, B.P., Benitez-Nelson, C.R., Hannides, C. C.S., Close, H.G., Drazen, J.C., Popp, B.N., 2020. Deep zooplankton rely on small particles when particle fluxes are low. Limnol. Oceanogr. Lett. 5, 410–416. https://doi.org/10.1002/lol2.10163.
Schartup, A.T., Thackray, C.P.P., Qureshi, A., Dassuncao, C., Gillespie, K., Hanke, A., Sunderland, E.M., 2019. Climate change and overfishing increase neurotoxicant in marine predators. Nature 572, 648–650. https://www.nature.com/articles/s41586-019-1468-9.
Selin, N.E., 2009. Global biogeochemical cycling of mercury: a review. Annu. Rev. Environ. Resour. 34, 43–63. https://doi.org/10.1146/annurev.environ.051308.084314.
Siegel, D.A., Buesseler, K.O., Doney, S.C., Sailley, S.F., Behrenfeld, M.J., Boyd, P.W., 2014. Global assessment of ocean carbon export by combining satellite observations and food-web models. Glob. Biogeochem. Cycles 28, 181–196. https://doi.org/10.1002/2013GB004743.Received.
Siegel, D.A., Buesseler, K.O., Behrenfeld, M.J., Benitez-Nelson, C.R., Boss, E., Brzezinski, M.A., Burd, A., Carlson, C.A., D'Asaro, E.A., Doney, S.C., Perry, M.J., Stanley, R.H.R., Steinberg, D.K., 2016. Prediction of the export and fate of Global Ocean net primary production: the EXPORTS science plan. Front. Mar. Sci. 3, 1–10. https://doi.org/10.3389/fmars.2016.00022.
Steinberg, D.K., Mooy, B.A.S. Van, Buesseler, K.O., Hole, W., Boyd, P.W., Karl, D.M., 2008. Bacterial vs. zooplankton control of sinking particle flux in the ocean ' s twilight zone. Limnol. Oceanogr. 53, 1327–1338.
Streets, D.G., Horowitz, H.M., Lu, Z., Levin, L., Thackray, C.P., Sunderland, E.M., 2019. Five hundred years of anthropogenic mercury: spatial and temporal release profiles. Environ. Res. Lett. 14 https://doi.org/10.1088/1748-9326/ab281f.
Sun, R., Sonke, J.E., Heimbürger, L.E., Belkin, H.E., Liu, G., Shome, D., Cukrowska, E., Liousse, C., Pokrovsky, O.S., Streets, D.G., 2014. Mercury stable isotope signatures of world coal deposits and historical coal combustion emissions. Environ. Sci. Technol. 48, 7660–7668. https://doi.org/10.1021/es501208a.
Sun, R., Yuan, J., Sonke, J.E., Zhang, Y., Zhang, T., Zheng, W., Chen, S., Meng, M., Chen, J., Liu, Y., Peng, X., Liu, C., 2020. Methylmercury produced in upper oceans accumulates in deep Mariana trench fauna. Nat. Commun. 11, 1–9. https://doi.org/10.1038/s41467-020-17045-3.
Sunderland, E.M., Krabbenhoft, D.P., Moreau, J.W., Strode, S.A., Landing, W.M., 2009. Mercury sources, distribution, and bioavailability in the North Pacific Ocean: insights from data and models. Glob. Biogeochem. Cycles 23, 1–14. https://doi.org/10.1029/2008GB003425.
Sunderland, E.M., Li, M., Bullard, K., 2018. Decadal changes in the edible supply of seafood and methylmercury exposure in the United States. Environ. Health Perspect. 126, 029003 https://doi.org/10.1289/EHP3460.
Tesan Onrubia, J.A., Petrova, M.V., Puigcorbe, V., Black, E.E., Valk, O., Hamelin, B., Buesseler, K.O., Masque, P., Le Moigne, F.A.C., Sonke, J.E., Rutgers van der Loeff, M., Heimburger-Boavida, L.-E., 2020. Mercury export flux in the Arctic Ocean estimated from 234Th/238U disequilibria. ACS Earth Sp. Chemi stry 4, 795–801. https://doi.org/10.1021/acsearthspacechem.0c00055.
Umhau, B.P., Benitez-Nelson, C.R., Close, H.G., Hannides, C.C.S., Motta, L., Popp, B.N., Blum, J.D., Drazen, J., 2019. Seasonal and spatial changes in carbon and nitrogen fluxes estimated using 234Th : 238U disequilibria in the North Pacific tropical and subtropical gyre. Mar. Chem. 217 https://doi.org/10.1016/j.marchem.2019.103705.
Volk, T., Hoffert, M.I., 1985. Ocean carbon pumps: Analysis of relative strengths and efficiencies in ocean-driven atmospheric CO2 changes. In: Sundquist, D., Broecker, W. (Eds.), The Carbon Cycle and Atmospheric CO2: Natural Variations Archean to Present. American Geophysical Union, pp. 99–110.
Washburn, S.J., Blum, J.D., Donovan, P.M., Singer, M.B., 2019. Isotopic evidence for mercury photoreduction and retention on particles in surface waters of Central California, USA. Sci. Total Environ. 674, 451–461. https://doi.org/10.1016/j.scitotenv.2019.04.145.
Weinstein, S.E., Moran, S.B., 2005. Vertical Flux of Particulate Al, Fe, Pb, and Ba from the Upper Ocean Estimated from $^{234}Th/^{238}U$ Disequilibria. Deep. Res. Part I Oceanogr. Res. Pap. https://doi.org/10.1016/j.dsr.2005.03.008.
Zhang, Y., Song, Z., Huang, S., P., Zhang, Y., Peng, P., Wu, J., Gu, S., Dutkiewicz, H., Zhang, S., Wu, F., Wang, L., Chen, S., Wang, Li, P, 2021. Global health effects of future atmospheric mercury emissions. Nat. Commun. 12, 3035 doi.org/10.1038/s41467-021-23391-7.